Impact of the mixing boundary layer on the relationship between PM2.5 and aerosol optical thickness

Neda Boyouk, Jean-François Léon, Hervé Delbarre, T. Podvin, C. Deroo

▶ **To cite this version:**

Neda Boyouk, Jean-François Léon, Hervé Delbarre, T. Podvin, C. Deroo. Impact of the mixing boundary layer on the relationship between PM2.5 and aerosol optical thickness. Atmospheric Environment, 2010, 44 (2), pp.271 - 277. 10.1016/j.atmosenv.2009.06.053 . hal-04437923

HAL Id: hal-04437923
https://hal.science/hal-04437923v1

Submitted on 5 Feb 2024

HAL is a multi-disciplinary open access archive for the deposit and dissemination of scientific research documents, whether they are published or not. The documents may come from teaching and research institutions in France or abroad, or from public or private research centers.

L'archive ouverte pluridisciplinaire **HAL**, est destinée au dépôt et à la diffusion de documents scientifiques de niveau recherche, publiés ou non, émanant des établissements d'enseignement et de recherche français ou étrangers, des laboratoires publics ou privés.

Impact of the mixing boundary layer on the relationship between PM2.5 and aerosol optical thickness

Boyouk Neda[1], Jean- François Léon[1*] and Hervé Delbarre[2], T. Podvin[1], C. Deroo[1]

1. Laboratoire d'Optique Atmospherique, CNRS –Université des sciences et technologies de Lille 1, Villeneuve d'Ascq, France

2. Laboratoire de Physico-Chimie de l'Atmosphère, CNRS-Université du Littoral Côte d'Opale, Dunkerque, France

*now at : Laboratoire d'Aérologie, CNRS-Université Paul Sabatier, Toulouse, France.

Key word: Mass concentration, Aerosol optical thickness, Boundary layer, lidar

Abstract

The purpose of this paper is to study the relationship between columnar aerosol optical thickness and ground-level aerosol mass. A set of Sun photometer, elastic backscattering lidar and TEOM measurements were acquired during April 2007 in Lille, France. The PM2.5 in the mixed boundary layer is estimated using the lidar signal, aerosol optical thickness, or columnar integrated Sun photometer size distribution and compared to the ground-level station measurements. The lidar signal recorded in the lowest level (240 m) is well correlated to the PM2.5 (R^2 = 0.84). We also show that the correlation between AOT-derived and measured PM2.5 is significantly improved when considering the mixed boundary layer height derived from the lidar. The use of the Sun photometer aerosol fine fraction volume does not improve the correlation.

1. Introduction

Most of the pollution aerosols emitted in the atmosphere are released in the atmospheric boundary layer and then become gradually dispersed and mixed through convection and turbulence. In addition to boundary layer features (e.g. depth, turbulent flux) that are key to understanding of the impact of aerosol on air quality, aerosol mass concentration measurements by air quality monitoring networks help to understand the dispersion of aerosols confined within the boundary layer. However, the aerosol vertical distribution and its temporal evolution are also of primary importance to understanding of changes in the aerosol mass concentrations at ground level, and to better characterize the distribution between local pollution events and large scale transport. In addition to ground-level observations, lidar vertical soundings provide a detailed description of scattering aerosols in the atmosphere. Primary parameters derived from elastic backscattering lidar profiles are the vertical distribution of aerosol backscattering and extinction coefficients. The vertical structure of the atmosphere can be inferred from a change in the backscattering vertical profile. Because the mixed layer has in general a higher aerosol backscattering coefficient than the free troposphere, the lidar can also detect the boundary between the two layers (Menut et al., 1999).

The relationship between aerosol mass and optical properties depends on the chemical composition, size and shape of the particles. Many studies (Chu et al., 2003; Gupta et al., 2006 ; Kacenelenbogen et al., 2006; Liu et al., 2004 ; Pelletier et al., 2007 ; Schaap et al., 2008 ; Wang and Christopher, 2003) have been devoted to finding the relationship between the columnar aerosol optical thickness (AOT) and the mass fraction PM2.5 or

PM10. The PM data can be derived from AOT measurements using a simple linear model (Chu et al., 2003; Kacenelenbogen et al., 2006; Wang and Christopher, 2003). However, the relationship depends on the season and on the site location. There are auxiliary parameters such as meteorological variables or the characteristics of the mixing layer that need to be accounted for (Pelletier et al., 2007). Liu et al. (2004) and Van Donkelaar et al. (2006) improved the capability of the multi angles imaging spectroradiometer-derived AOT in estimating surface level PM2.5 by using aerosol vertical profiles simulated by a global atmospheric chemistry model. This result suggests that the use of vertical information, namely the altitude of the mixed layer or the aerosol extinction profile can improve the determination of PM from AOT measurements. Gupta et al.(2006) highlighted the impact of the mixing height on the relationship between AOT and PM2.5. From their dataset over Texas, they found that the best correlation between PM2.5 and AOT is seen when the mixing height is between 100 and 200 m and when the relative humidity is less than 50%. However Schaap et al.(2008) did not find a significant improvement in the correlation between AOT and PM when including the lidar-derived mixing layer height in their study in the Netherlands. However they found that the PM2.5-AOT correlation increased when the comparison time slot was centred around and on noon, which suggests that the aerosols were well mixed in the boundary layer. The relative humidity also had an impact on the AOT via an increase in the size of the particles and a change in the refractive index (Hänel, 1976). Shinozuka et al. (2007) found that the fraction of ambient AOT due to water uptake was 37 % ± 15% during their field campaign in North America. The change in aerosol scattering or extinction as a function of relative humidity can be parameterized (Kotchenruther and Hobbs, 1998 ; Raut and Chazette, 2007) but in most cases the relative humidity vertical profile and the aerosol hygroscopic properties remains unknown.

In this paper, we present observations performed at an urban site in the North of France. The experimental site is located on the outskirt of the city of Lille, France. Lille (50.61°N, 3.14°E) is a conurbation of 1.2 million inhabitants and in the vicinity of many urban and industrial aerosol pollution sources. We present the study of a pollution event that occurred during the month of April 2007. In March and April 2007, daily PM10 concentrations often exceeded 50 $\mu g.m^{-3}$ corresponding to the European-24 hours limit that must not to be exceeded on more than 35 days per year. The pollution events were also observed by Schaap et al.(2008) at Cabauw, The Netherlands. This period was chosen according to the availability of data for all of the instruments that were used in this study. We analyze the evolution of the aerosol mass at the ground in conjunction with lidar soundings and Sun photometer measurements. The objective is to analyze the built-up and removal of the aerosol load during the pollution event and to assess the variation in the relationship between aerosol mass at the ground and aerosol optical thickness.

2. Data and Methods

2.1. Ground-level measurement of the particulate mass concentration

During the last decades a number of epidemiological studies have shown a link between pollution by airborne particulate matter (PM) and respiratory and cardiovascular diseases either for short-term or long-term exposure (Dockery et al., 1993; Künzly et al., 2000; Pope III et al., 1995). The particle mass concentration measured at ground level is a way to evaluate the impact of aerosols on air quality. PMX means the mass concentration of

particles with an aerodynamic diameter lower than X. In the present study we are using PM2.5 and PM10 data collected by a Tapering Element Oscillation Microbalance TEOM (Patashnick and Rupprecht, 1991) operated by the regional air quality network ATMO Nord-Pas de Calais. The measurement site is located downtown Lille (Faidherbe street) at less than 3 km from the lidar site at Université des Sciences et Technologies de Lille. Comparisons of TEOM to gravimetric measurements (Allen and Ress, 1997; Van Dingenen et al., 2004) show that routine TEOMs can underestimate PM10 by up to 35%. As this TEOM is not equipped with a Filter dynamics measurement system (FDMS), we have to apply a so-called correction factor on our PM10 and PM2.5 measurements. This factor is provided by air quality network ATMO Nord-Pas de Calais, and used for PM10. The factor is derived from a systematic comparison with data acquired by two other TEOM-FDMS located in the administrative area Nord-Pas de Calais (Calais and Tourcoing). During the experimental period, the PM2.5 was not measured with the TEOM-FDMS, so the correction factor for PM2.5 remains unknown. Since May 2008, the PM2.5 is also monitored by a TEOM-FDMS. We have compared the correction factor used for PM10 and for PM2.5 for the last ten days of May 2008, corresponding to a similar meteorological situation for our observation period. Both correction factors are well correlated (R=0.95) and the PM2.5 correction factor can be derived from the PM10 one by using a linear relationship:

$$PM2.5_{corrected} = PM2.5 \times (\frac{PM10_{corrected}}{PM10} - 0.1) \times 1.25 \quad (1)$$

In this regression, we have only considered PM10 higher than 10µg/m^3.

2.2. Columnar integrated aerosol optical properties using Sun photometer

We have used the data collected by a sky-scanning ground-based automated Sun photometer (referred in the AERONET data base as Lille) belonging to the Aerosol Robotic Network (Holben et al., 1998). A full description of the instrument and the retrieval procedure can be found in Holben et al.(1998) and Dubovik et al. (2000). The primary parameter that can be derived from the Sun photometer is the aerosol optical thickness (AOT) at four wavelengths (440, 670, 870, 1020 nm) and with an absolute uncertainty of ~0.010-0.021 (Holben et al., 2001). To be coherent with the lidar wavelength, we interpolate the AOT at 532 nm according to the Angström law and using the channels at 440 and 670 nm.

The columnar integrated volume size distribution dV/dlnr (in $\mu m^3/\mu m^2$) in range of radii between 0.05 and 15 μm is also derived from sky brightness measurements (Dubovik and King, 2000). The retrieval of particle volume size distribution was demonstrated to be adequate in practically all situations (Dubovik et al., 2002). The error in the retrieved volume density changes as a non-linear function of particle size, aerosol type and actual values of size distribution. In particular, for the intermediate size particle size range 0.1 and 7.0 μm, the retrieval errors do not exceed 10% in the maximum of size distribution and may increase up to 35% for the points corresponding to the minimum values of size in this size range. The retrieved size distribution volume is not independent in the sense that the retrieval technique insures only the fact that the retrieved combination of all of the parameters would accurately reproduce the measured radiation field in the scope of chosen radiative transfer model.

2.3. Vertical profile of aerosol observed by lidar

We have used an aerosol micropulse Lidar manufactured by CIMEL (Pelon et al., 2008).. It uses a Q-switched frequency-doubled ND:YAG laser with an expanded beam (8-10 μJ with a 200 mm exit-lens diameter) and a pulse repetition frequency of 4.7 kHz. The wavelength is 532 nm. During a 10 min data acquisition sequence, 10 individual profiles are acquired and averaged. Then the system waits for 20 min before starting another acquisition sequence. The duration of a pulse is 100 ns leading to a vertical resolution of 15 m. The profiles are averaged to reduce the influence of background noise. During the day time the background noise is dominated by direct or scattered sunlight causing a sharp decrease in the signal-to-noise ratio. The background noise is estimated by taking the average of the backscatter signal between 22 and 30 km, then subtracting it before evaluating the signal. The data processing includes the correction of the spurious signal due to the detection of the scattered light in the receiver, called the afterpulse signal and the correction of the overlap function (Pelon et al., 2008). The Lidar backscatter signals are calibrated for a reference altitude in which the particle backscatter coefficient is negligible compared to the known molecular backscatter. In this study the reference altitude is between 4 ~ 4.5 km on cloud-free days. Because of the after pulse the attenuated backscatter coefficients are not useful between 0 and 225 m.

We compute the aerosol extinction and backscatter coefficient using the Klett method (Klett, 1981) that requires a given lidar ratio. Using Raman lidar, *Ansmann and Müller* (2005) have given a range of lidar ratio between 35 and 70 sr at 532 nm for less absorbing urban aerosols (Ansmann et al., 2001; Franke et al., 2001). The lidar ratio can be estimated using the aerosol scattering phase function and single scattering albedo derived from the Sun photometer using:

$$L_{aer} = \frac{4\pi}{\omega_0 P(180)} \quad (2)$$

Where ω_0 is the single scattering albedo and P(180) is the backscattering phase function. Using this approach, *Cattral et al.* (2005) have estimated that the lidar ratio for urban/industrial pollution is 71 sr. Lidar ratio value is obtained by linear interpolation at 532 nm of AERONET retrieved phase function and single scattering albedo between 675 nm and 440 nm. We have estimated an average lidar ratio for the site of Lille of 67 sr with a standard deviation of ± 11 sr using 23 retrievals. This average value has been used throughout this study for determining the extinction coefficient.

The use of lidar data to detect the mixed layer top height or entrainment zone thickness has been widely investigated (Baars et al., 2008; Flamant et al., 1997; Lammert and Bösenberg, 2006 ; Menut et al., 1999 ; Seibert et al., 2000). The top of the mixed boundary layer (MBL) is detected using the modulus (absolute) of the minimum of the first derivative of the range corrected signal (Flamant et al., 1997). Indeed, a decrease in the range corrected lidar signal is observed in the transition zone between the aerosol loaded boundary layer and the free troposphere. We have then determined the altitude of the boundary layer by using a simple gradient method applied to the lidar profiles acquired during the day and night at a time resolution of 30 min.

2.4. Retrieval of ground-level PM2.5 from lidar and Sun photometer observations

We have explored the relationship between the ground-level aerosol mass concentration and the optical measurements acquired by the lidar and the Sun photometer using three

different methods based on a simple correlation analysis. First, the range corrected attenuated backscattered lidar signal $S(z_l)$ at the lowest available altitude can be used to infer the mass concentration close to the ground. The lidar signal is not available in the first hundred meters because of the afterpulse effect. We have estimated that the first level that can be used is at $z_l = 240$ m.

Secondly, we have compared the Sun photometer AOT with PM2.5. The relationship between columnar AOT and ground-level PM2.5 is not straightforward and depends on the vertical distribution and the optical, size distribution and hygroscopic properties of the aerosol. Under the basic assumption that the aerosol mass is well mixed in the boundary layer and that the relative humidity has a negligible impact on the extinction coefficient, we have computed the Sun Photometer derived PM2.5 using :

$$PM2.5_{AOT}^{Aeronet} = \frac{\tau}{\sigma^{*} H_{BL}} R_{BL} \qquad (3)$$

Where τ is the AOT derived from Sun photometer data, H_{BL} the MBL top and R_{BL} the lidar derived AOT ratio between the boundary layer and the total column. σ^{*} is the specific mass extinction coefficient. We took a value of 4.75m^2/g that is justified *a posteriori* to get a regression slope as close as possible to one. We have tested one after the other the impact of using H_{BL} and R_{BL}.

At last, we have considered the Sun photometer derived fine mode volume fraction as a better proxy for the PM2.5. We define $V_{1\mu m}$ the fine mode volume as

$$V_{1\mu m} = \int_{0.05\mu m}^{1\mu m} \frac{dV(r)}{d\ln r} d\ln r$$

(4)

The Sun photometer derived PM2.5 is then obtained given the following equation:

$$PM2.5_{Volume}^{AERONET} = \frac{\rho V_{1\mu m}}{H_{BL}}$$

(5)

ρ is the density of dry aerosol and we took ρ = 1.7 g/cm^3 (Sloane, 1984). During the observation period, the fine mode dominates the size distribution and have the major contribution to the AOT . Figure 1 shows that the fine mode volume fraction is well correlated with the total AOT as opposite to the total volume fraction. This latter parameter is not considered in the following of the study as it is poorly correlated with the ground-level PM2.5.

The errors and uncertainties are due to the inversion method used, calibration of the instruments and the difference in the time and space location of the different measurements. This latter error is probably the largest but remains extremely difficult to quantify. Using the first available level of the lidar signal, the error in estimating ground-level PM2.5 is proportional to the error in the lidar backscattered signal in the first hundred meters. Due to the overlap function, Pelon et al. (2008) have estimated that error in the lidar backscattered signal is ± 10% above 600 m and can be up ± 50% when the signal is extrapolated down to ground level. An additional source of error comes from the impact of the relative humidity on the aerosol optical properties. This impact can be modeled (Hänel, 1976) when the aerosol type (hygroscopic factor) and the vertical profile of relative humidity are known (Raut and Chazette, 2008). Since we have the relative

humidity measured at the ground, we have only applied a correction factor for the lidar signal by defining a corrected signal $S^*(z_l)$:

$$S^*(z_l) = S(z_l) * (1 - RH)^{0.55} \quad (6)$$

where RH is the relative humidity and z_l is the lowest valuable level. Eq. 6 stems from a modeling of the scattering cross section and size growth factor due to water uptake (Hänel, 1976). This equation is only applied here at the lowest level of the lidar measurements (zl=240 m). Within such a short range, the lidar signal is proportional to the lidar backscattering at the first order so the dependence of the scattering cross section with relative humidity (depicted in Hänel, 1976) is well appropriate. The exponent factor 0.55 has been chosen by optimizing the final correlation factor between the lidar retrieved PM2.5 and ground PM2.5 measurements, and is found to be close to the value in Raut and Chazette (2007). The overall uncertainty is between 20 and 40%.

In equation (3), the error in the retrieved mass is proportional to the error in τ, H_{BL}, R_{BL}, and σ^*. Calibration accuracy causes instrumental error of 0.01 in τ which is in the order of 5 to 10% of optical thickness for $\tau_{aer}(440) \leq 0.2$. The estimation of H_{BL} was manually checked and the relative error was ~5%. R_{BL} uncertainty depends on the error in the retrieved extinction profiles, which depends on the choice of the lidar ratio. Considering the lidar ratio variability given in paragraph 2, we have estimated the uncertainty of R_{BL} to be 30-40%. However, as we use a constant lidar ratio, this error can be larger. As we have used a constant value for σ^*, a change in the aerosol type will introduce significant error to the estimation. However, we consider a relatively short period of time (less than 1 month) which was dominated by fine pollution particles and we have estimated the error to be ~10%, the same as the error in the density. Considering equation (5),it can be seen

that the use of the fine mode aerosol volume fraction introduces an error due to its retrieval of ~15% (Dubovik et al., 2000). However, the error can be much larger (up to 100%) when the coarse mode dominates the size distribution, which is not the case during our observation period.

3. Results

3.1. Evolution of aerosol mass, optical thickness and mixed boundary layer height.

Figure 2 shows the daily average variation of PM2.5 and AOT during April 2007. We can observe a sharp increase in AOT and PM2.5 between 7 and 13 April and a second increase between 25 and 28 April. Our lidar data set begins on April 13, 2007. The daily average PM2.5 value starts from less than 18 $\mu g/m^3$ on April 7 and reaches 62$\mu g/m^3$ on April 13. The AOT changes from 0.1 to 0.6 in the same time. From the 18 to the 25 April, the daily average PM2.5 is between 15 and 22$\mu g/m^3$ and on average the AOT is 0.3. A second increase is observed at the end of the month with a maximum in PM2.5 on 27 April (45 $\mu g/m^3$) and a corresponding daily average AOT of 0.5. The maximum in AOT is reached on 28 April. We have based our study on the hourly data and we have selected the hours for which all the necessary data (lidar profiles, Sun photometer inversions and PM2.5 measurements) were available. The lidar system was stopped between 12 April 07:00 and 13 April 07:00 UTC for maintenance so we considered the lidar data since 13 April. The data set includes measurements acquired on April 14 to 22 and on April 26, 27 and 30.

During the observation period, a ridge of high pressure dominates over Europe until mid-April and is then slightly perturbed by northern and eastern low-pressure areas. This scheme ensures a fine weather with clear skies over the region before April 17 and some elevated clouds after, which are well detected in the lidar profiles. Temperature time series show respectively a clear diurnal cycle from 10 to 25°C and from 5 to 15°C before and after 17 April. Northerly air masses during this period are characterized by a low wind speed (<5 m/s) at the ground level, mainly driven by turbulent momentum transfer. The MBL development is then systematically associated with an increase in wind speed in the morning, which highlights the turbulent activity. Solar radiation ranges from 550 W/m^2 (cloudy days) to 750 W/m^2 (clear sky) in the area. Such wind speed and solar radiation ensure a highly or moderately unstable atmosphere during convective periods, according to the Pasquill classification. The MBL dynamics retrieved from lidar signal fit well with humidity and wind time series. This analysis particularly shows that fog is a major local phenomenon before 17 April and after 25 April, which delays the boundary layer development by a few hours. This feature is illustrated on Figure 3 showing the diurnal development of the MBL (between 8:00 and 18:00 UTC) for 15 and 21 April. The complete daily cycle of the MBL height is illustrated on Figure 4 along with the variation of the logarithm of the range corrected attenuated backscattering coefficient between 15 and 16 of April and between 21 and 22 April, 2007. The panels illustrate the diurnal variability in the vertical structure of the atmosphere. We can observe significantly higher value of the backscattering coefficient close to the ground level during the first period (Figure 4a). The white color shows missing data on April 15 in the early morning due to condensation of water on the optical system. The urban boundary layer has a complicated three-dimensional structure which is difficult to describe comprehensively. Fine resolution of time- height lidar data is useful to reveal the daily cycle of convective

boundary layer growth and collapse. The mixing layer height depends on the meteorological conditions and other primary factors: wind speed and buoyant forcing (convection) due to solar heating of the surface (Stull, 1988). On 15 April (Figure 4a), we can observe three different aerosol layers between 9:00 and 15:00 UTC. The bottom layer corresponds to the mixed boundary layer (black dots) that increases in height in the morning and the early afternoon and collapse in the late afternoon (17:00-18:00 UTC) to form the nocturnal boundary layer (also observed on 16 April). The residual layer is observed in the morning and during the night with a top height at 1.3-1.4 km. During the period of low PM2.5 and AOT (21-22 April, see Figure 4b), the MBL height diurnal cycle is clearly smoother. We can also observe an aloft layer up to 3 km during the beginning and the end of the observation period that disappears during the period of low PM2.5 and AOT. This feature is presented in Figure 5 which shows the retrieval of the aerosol extinction coefficient on 15 and 21 of April at 16:00 UTC and 26 at 17:00 UTC. This aloft layer appears after 17:00 UTC on April 13, 5 hours after the maximum aerosol concentration measured at ground level. During the build-up of the pollution event, the wind direction at the ground level is North-East. Air mass back-trajectories (not shown) computed for 13 April confirms the eastward continental origin of the air mass. The wind direction moved to the North and North-West after 13 April bringing air mass from the North Sea. The presence of the aloft layer affects the AOT ratio between the MBL and the total column, R_{BL}. It is 44.6% on 15 April, 72.8% on 21 April and 33.1% on 26 April, 2007.

3.2. Retrieval of ground-level PM2.5

Comparison between ground-level PM2.5 and retrieved PM2.5 has been shown on Figure 6. According our methods we have used the fine volume fraction (V-H) or the AOT (AOT-H) corrected for the MBL height, and the lidar signal at 240m (S-RH) corrected for relative

humidity effect. The results of the comparison is summarised in Table 1. The lidar signal in the lowest level is well correlated with the ground-level PM2.5. The regression is adjusted to have a slope close to 1. The correction for relative humidity impact increases the correlation ($R^2 = 0.84$). The total AOT is also correlated to ground-level PM2.5. There is a significant improvement in the relationship (correlation, regression coefficient and RMSE) when the MBL height is accounted for. However, we cannot observe any improvement when we consider the AOT ratio between the MBL and the total column. The uncertainty of this parameter remains high because it depends on the lidar ratio vertical profile. Moreover, there is a clear impact of the relative humidity profile in the MBL that is not currently accounted for. Using the fine mode volume fraction instead of total AOT does not significantly improve the relationship. The AOT is directly measured with excellent accuracy, whilst accuracy of the fine volume fraction retrieval primarily depends on AOT and contributions from the coarse mode. Considering the use of AOT and MBL height, the remaining offset is ~12 $\mu g/m^3$. This offset can be attributed to the distance gap between the ground station and the Sun photometer which is crucial when considering low AOT and mass concentration. Moreover, equation (1) is not valid for low aerosol concentration that may correspond to situation with a significant contribution from volatile compounds.

4. Conclusion

We have performed ground-based measurements in the North of France (Lille, 50.61°N, 3.14°E) to analyze the relationship between the aerosol optical thickness and the mass concentration at the ground. A set of backscattering lidar soundings, ground-level aerosol mass concentration along with Sun photometer observations were acquired during the month of April 2007. During this period, the aerosol mass concentrations were highly

variable with AOT between 0.11 and 0.66 (at 532 nm) and PM2.5 between 2 and 65 $\mu g/m^3$. Lidar analysis reveals also a large variability in the MBL height diurnal cycle and in the aerosol extinction vertical distribution. The lidar backscattering coefficient at the lowest possible level is well correlated to the ground-level PM2.5. When considering the total aerosol optical thickness, we obtain a fairly good estimate of the PM2.5 at the ground-level under the assumption that the MBL height is known. As the AOT is the primary parameter derived from aerosol satellite measurements (King et al., 1999), the relationship between AOT and ground-level mass concentration has a crucial importance for the monitoring of aerosol pollution from space. Using the Sun photometer retrieved aerosol fine mode volume concentration did not improve the correlation with PM2.5. Moreover we did not improve this relationship by using the AOT ratio between the MBL and the total column. However this parameter depends on the lidar ratio profile that cannot be determined using a single wavelength backscatter lidar. The proposed approach will benefit from additional observations including different aerosol types and meteorological situations. Further improvements on the overall accuracy of the method are also expected from a dedicated aerosol optical properties joint retrieval between combined Sun photometer and lidar observations.

References:

G. Allen and R. Ress, Evaluation o the TEOM method for measurement of ambiant particulate mass in urban areas, *J. Air Waste Manage. Assoc.* **47**(1997), pp. 682-689.

A. Ansmann and D. Müller, Lidar and atmospheric aerosol particle. In: C. Weitkamp, Editor, *LIDAR: Range resolved optical remote sensing of the atmosphere*, Springer, Geessthacht, Germany (2005), pp. 105-141.

A. Ansmann *et al.*, European pollution outbreaks during ACE 2: lofted aerosol plumes observed with Raman lidar at the Portuguese coast, *J. Geophys. Res.* **106**(2001), pp. 20,725-720,733.

H. Baars, A. Ansmann, R. Engelmann and D. Althausen, Continuous monitoring of the boundary-layer top with lidar, *Atmos. Chem. Phys.* **8**(2008), pp. 7281-7296.

C. Cattrall, J. Reagan, K. Thome and O. Dubovik, Variability of aerosol and spectral lidar and backscatter and extinction ratios of key aerosol types dervied from selected Aerosol Robotic Network locations, *J. Geophys. Res.* **110**(2005).

D.A. Chu *et al.*, Global monitoring of air pollution over land from the Earth observing system-Terra Moderate imaging spectroradiometer (MODIS), *J. Geophys. Res.* **108**(2003), p. 4661.

D.W. Dockery *et al.*, An association between air pollution and mortality in Six U.S. cities, *The New England Journal of Medicine* **329**(1993).

O. Dubovik *et al.*, Variability of absorption and optical properties of key aerosol types observed in worldwide locations, *J. Atmos. Sci.* **59**(2002), pp. 590-608.

O. Dubovik and M.D. King, A flexible inversion algorithm for retrieval of aerosol optical properties from sun and sky radiance measurements, *J. Geophys. Res.* **105**(2000), pp. 20,673-620,696.

O. Dubovik *et al.*, Accuracy assessments of aerosol optical properties retrieved from Aerosol Robotic Network (AERONET) Sun and Sky radiance measurements, *J. Geophys. Res.* **105**(2000), pp. 9791-9806.

C. Flamant, J. Pelon, P.H. Flamant and P. Durand, Lidar determination of the entrainment zone thickness at the top of the unstable marine atmospheric boundary layer, *Boundary-Layer Meteorol.* **83**(1997), pp. 247-284.

K. Franke *et al.*, One-year observations of particle lidar ratio over the tropical Indian Ocean with Raman lidar, *Geophys. Res. Lett.* **28**(2001), pp. 4559-4562.

P. Gupta *et al.*, Satellite remote sensing of particulate matter and air quality assessment over global cities, *Atmos. Environ.* **40**(2006), pp. 5880-5892.

G. Hänel, The properties of atmospheric aerosol particles as functions of the relative humidity at thermodynamic equilibrium with surrounding moist air, *Adv. in Geophys.* **19**(1976), pp. 73-188.

B.N. Holben *et al.*, AERONET-A federated instrument network and data archive for aerosol characterisation, *Rem. Sens. Environ.* **66**(1998), pp. 1-16.

B.N. Holben *et al.*, An emerging ground-based aerosol climatology: Aerosol optical depth from AERONET, *J. Geophys. Res.* **106**(2001), pp. 12,067-012,097.

M. Kacenelenbogen, J.-F. Léon, I. Chiapello and D. Tanré, Characterization of aerosol pollution events in France using ground-based and POLDER-2 satellite data, *Atmos. Chem. Phys.* **6**(2006), pp. 4843-4848-4849.

M.D. King, Y.J. Kaufman, D. Tanré and T. Nakajima, Remote sensing of tropospheric aerosols from space: past present and future, *Bull. Amer. Meteor. Soc.* **80**(1999), pp. 2229-2259.

R.A. Kotchenruther and P.V. Hobbs, Humidification factors of aerosols from biomass burning in Brazil, *J. Geophys. Res.* **103**(1998), pp. 32081-32089.

N. Künzly *et al.*, Public-health impact of outdoor and traffic-related air pollution: a European assessment, *The Lancet* **356**(2000), pp. 795-801.

A. Lammert and J. Bösenberg, Determination of the convective boundary layer height with laser remote sensing, *Boundary-Layer Meteorol.* **119**(2006), pp. 159-170.

Y. Liu *et al.*, Mapping annual mean ground-level PM2.5 concentrations using multiangle imaging spectroradiometer aerosol optical thickness over the contiguous United States, *J. Geophys. Res.* **109**(2004).

L. Menut, C. Flamant, J. Pelon and P.H. Flamant, Urban boundary-layer height determination from lidar measurements over the Paris area, *Appl. Opt.* **38**(1999), pp. 945-954.

H. Patashnick and E.G. Rupprecht, Continuous PM10 measurements using the tapered element oscillating microbalance, *J. Air Waste Manage. Assoc.* **41**(1991), pp. 1079-1083.

B. Pelletier, R. Santer and J. Vidot, Retrieving of particulate matter from optical measurements: a semiparametric approach, *J. Geophys. Res.* **112**(2007).

J. Pelon *et al.*, Microlidar observations of biomass burning aerosol over Djougou (Benin) during African Monsoon Multidisciplinary Analysis Special Observation Period 0: Dust and Biomass Burning Experiment, *J. Geophys. Res.* **113**(2008).

C.A. Pope III, D.W. Dockery and J. Schwartz, Review of epidemiological evidence of health effects of particulate air pollution, *Inhalation Toxicology* **7**(1995), pp. 1-18.

J.C. Raut and P. Chazette, Retrieval of aerosol complex refractive index from a synergy between lidar, sunphotometer and in situ measurements during LISAIR experiment, *Atmos. Chem. Phys.* **7**(2007), pp. 2797-2815.

J.C. Raut and P. Chazette, Vertical profiles of urban aerosol complex refractive index in the frame of ESQUIF airborne measurements, *Atmos. Chem. Phys.* **8**(2008), pp. 901-919.

M. Schaap, A. Apituley, R.M.A. Timmermans, R.B.A. Koelemeijer and G. de Leeuw, Exploring the relation between aerosol optical depth and PM2.5 at Cabauw, the Netherlands, *Atmos. Chem. Phys.* **9**(2008), pp. 909-925.

P. Seibert *et al.*, Review and intercomparison of operational methods for the determination of the mixing height, *Atmos. Environ.* **34**(2000), pp. 1001-1027.

Y. Shinozuka *et al.*, Aircraft profiles of aerosol microphysics and optical properties over North America: Aerosol optical depth and its association with PM2.5 and water uptake, *J. Geophys. Res.* **112**(2007).

C.S. Sloane, Optical properties of aerosols of mixed composition, *Atmos. Env.* **18**(1984), pp. 871-878.

R.B. Stull, *An introduction to boundary layer meteorology* Kluwer Academic Publishers, Dordrecht (1988) 666 pp.

R. Van Dingenen, F. Raes and et al., A European aerosol phenomology - 1: physical characteristics of particulate matter at kerbside, urban, rural and background sites in Europe, *Atmos. Environ.* **38**(2004), pp. 2561-2577.

A. Van Donkelaar, R.V. Martin and R.J. Park, Estimating ground-level PM2.5 using aerosol optical depth determined from satellite remote sensing, *J. Geophys. Res.* **111**(2006).

J. Wang and S.A. Christopher, Intercomparison between satellite-derived aerosol optical thickness and PM2.5 mass: Implications for air quality studies, *Geophys. Res. Lett.* **30**(2003), p. 2095.

Table 1: Summary of the correlation study between ground level PM2.5 and the lidar signal (S) at 240 m, the lidar signal at 240 m with a correction for relative humidity impact (S-RH), the aerosol optical thickness (AOT), the AOT and the MBL height (AOT-H_{BL}), the AOT, MBL height and ratio of MBL AOT to total AOT, (AOT-HBL-RBL), and the fine mode volume fraction and MBL height (Vol-HBL). The uncertainties on the parameters derived from a least squared fit to a straight line model are given within the brackets.

	R^2	RMSE	Slope	intercep
S	0.80	10	1.0 (0.1)	34 (3)
S-RH	0.84	9	1.0 (0.1)	42 (3)
AOT	0.61	16	1.0 (0.2)	22 (5)
AOT-H_{BL}	0.73	12	1.0 (0.1)	10 (4)
AOT-H_{BL}–R_{BL}	0.56	15	0.8 (0.1)	28 (5)
Vol-H_{BL}	0.65	15	1.0 (0.1)	13 (5)

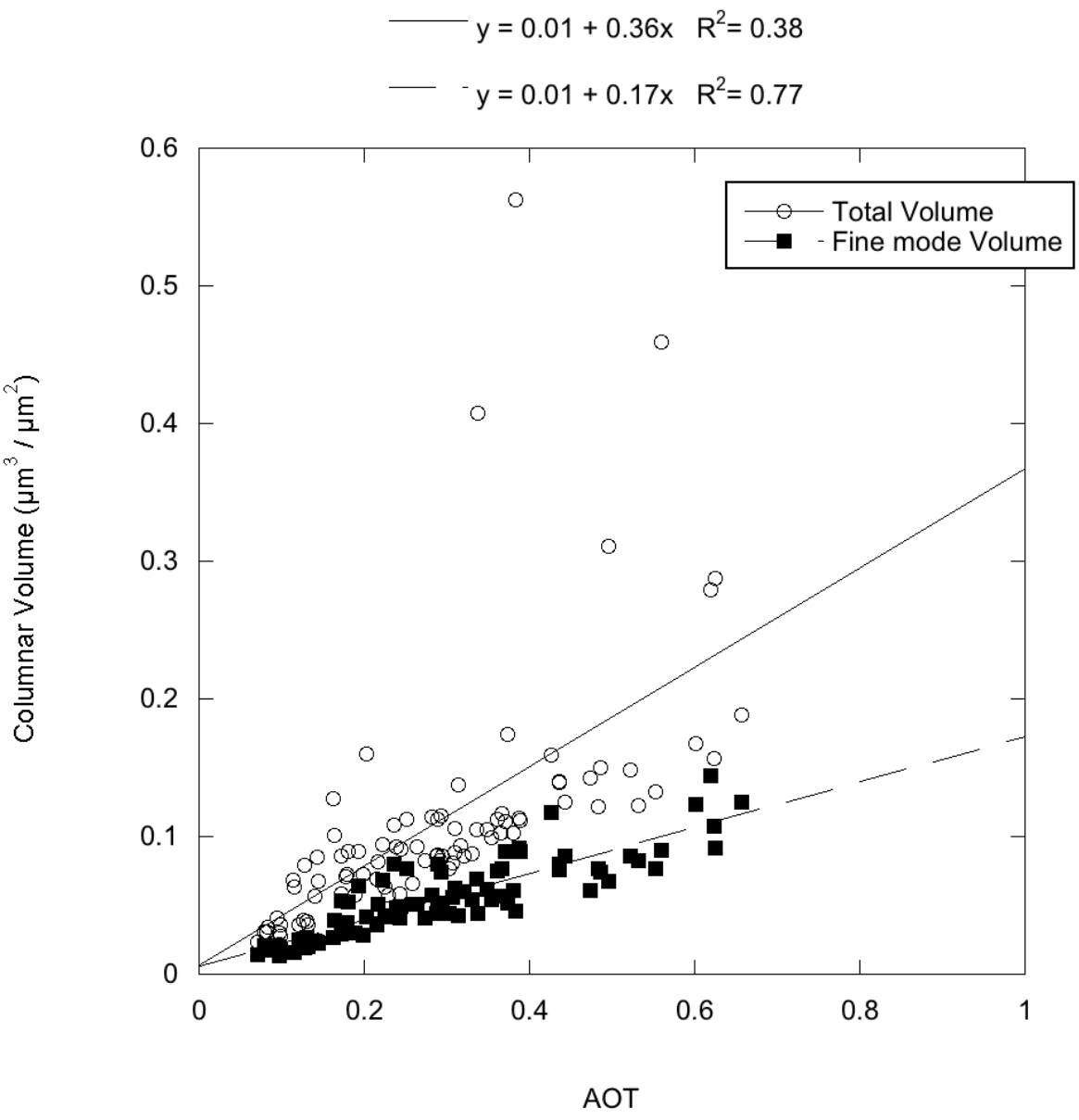

Figure1. Comparison between aerosol optical thickness and total and fine volume fraction (columnar integrated) derived from Sun photometer.

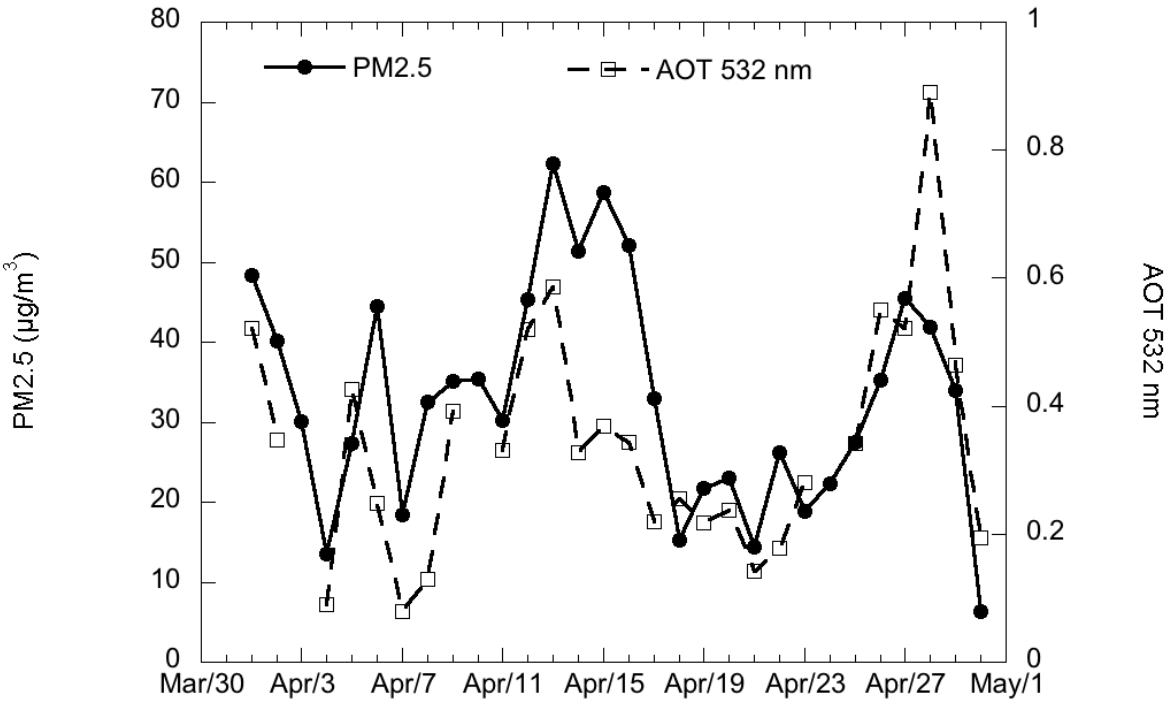

Figure 2. Daily average of PM2.5 and aerosol optical thickness during April 2007 in Lille.

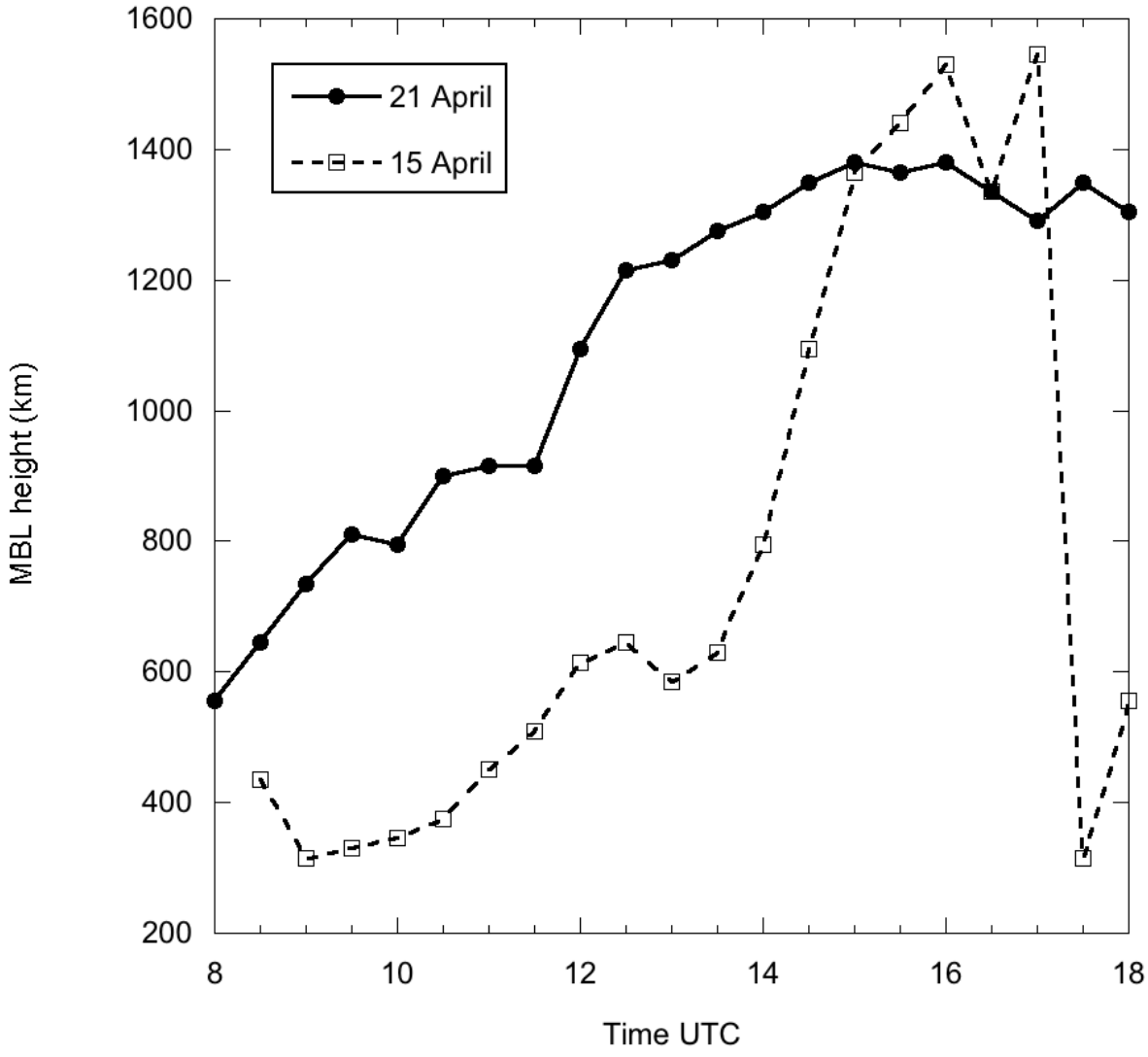

Figure 3. Top altitude of the mixed boundary layer for 15 April and 21 April. The time step is 30 min.

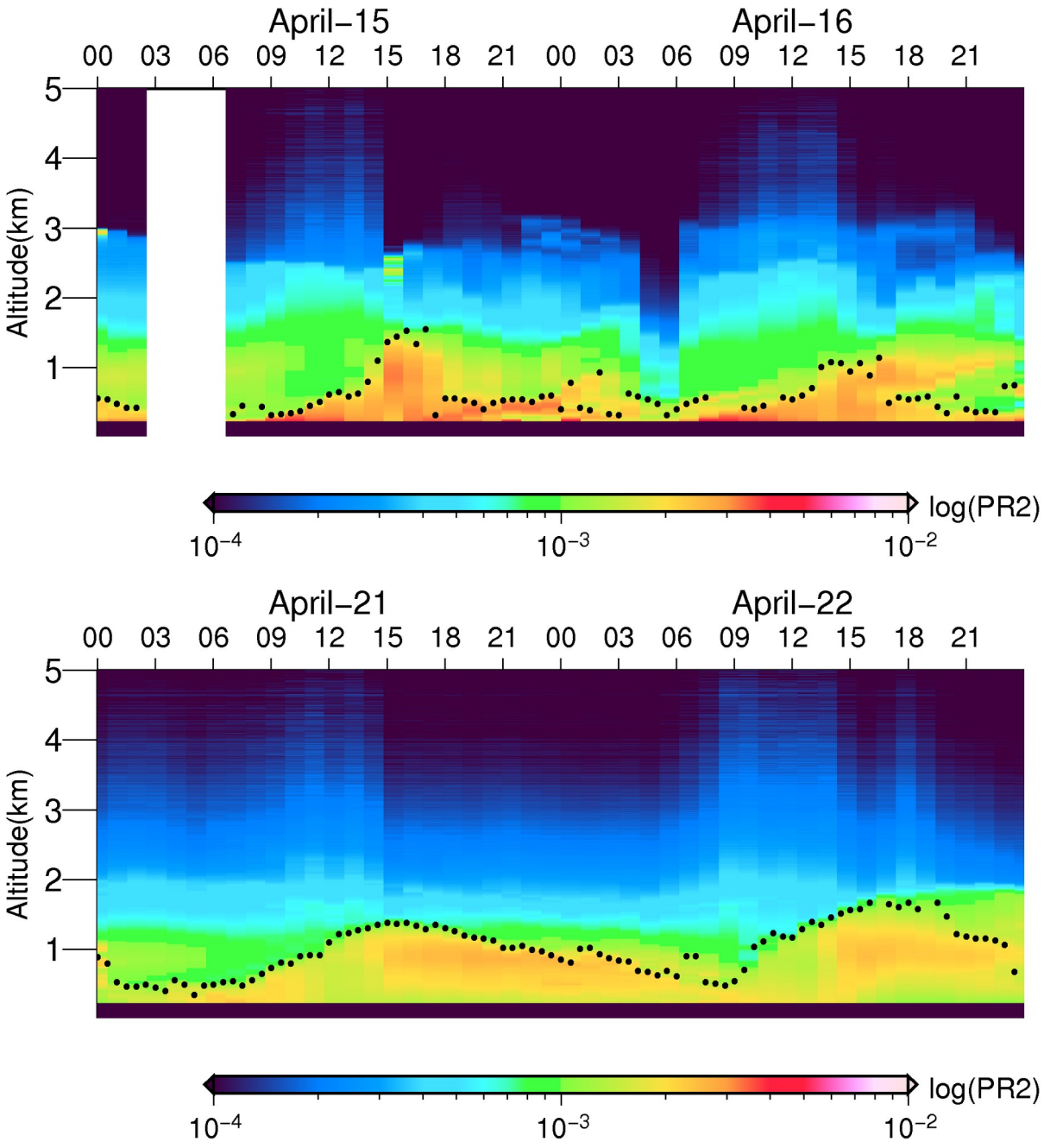

Figure 4. Logarithm of the range corrected lidar signal for (top) April 15 to 16 and for (bottom) April 21 to 22 2007. The time step is 30 min. The black dots are located at the top of the mixed boundary layer.

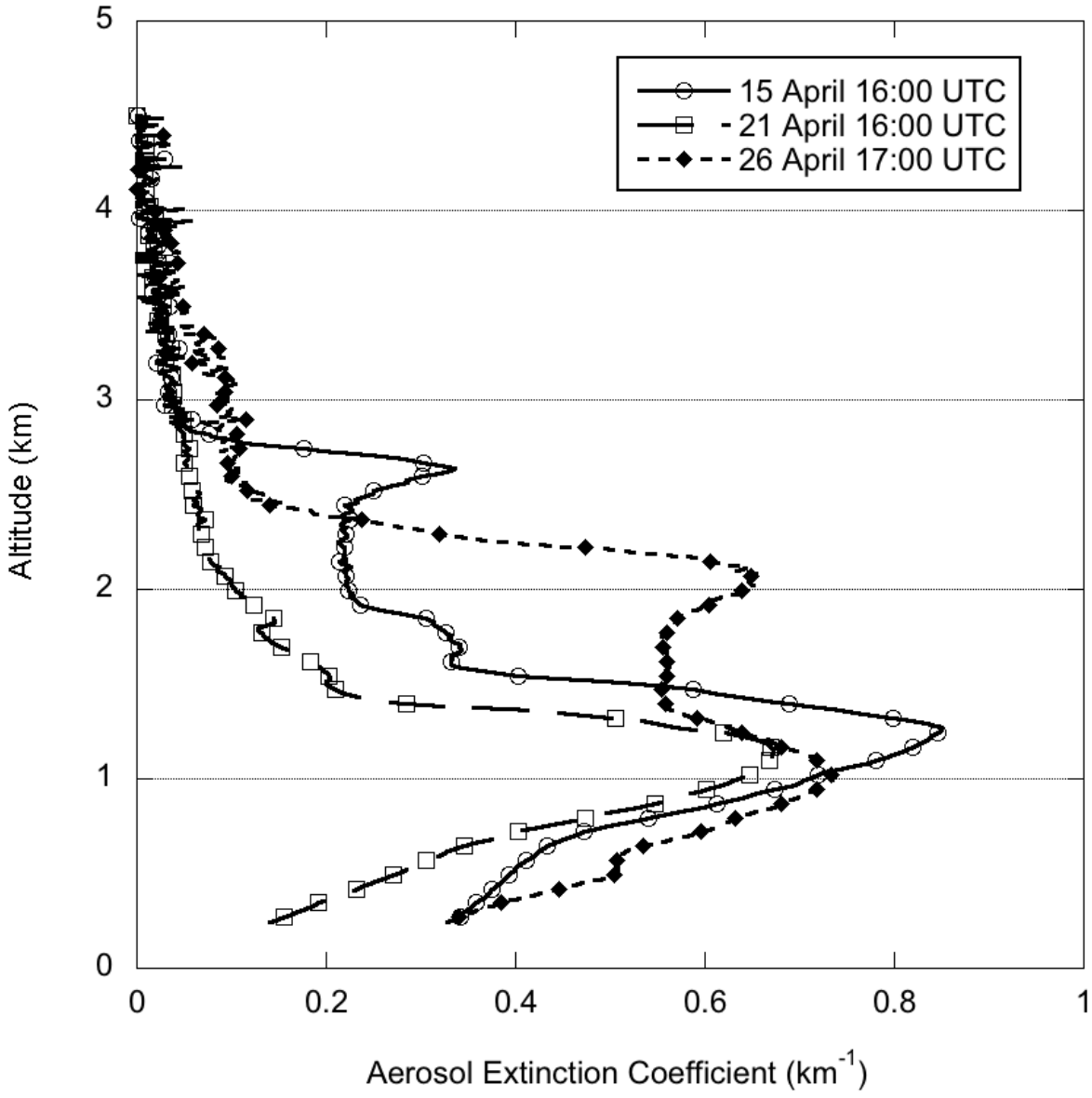

Figure 5. Vertical profile of aerosol extinction coefficient at 532 nm on April 15 and 21 at, 2007 at 16:00 UTC and April 26, 2007 at 17:00 UTC.

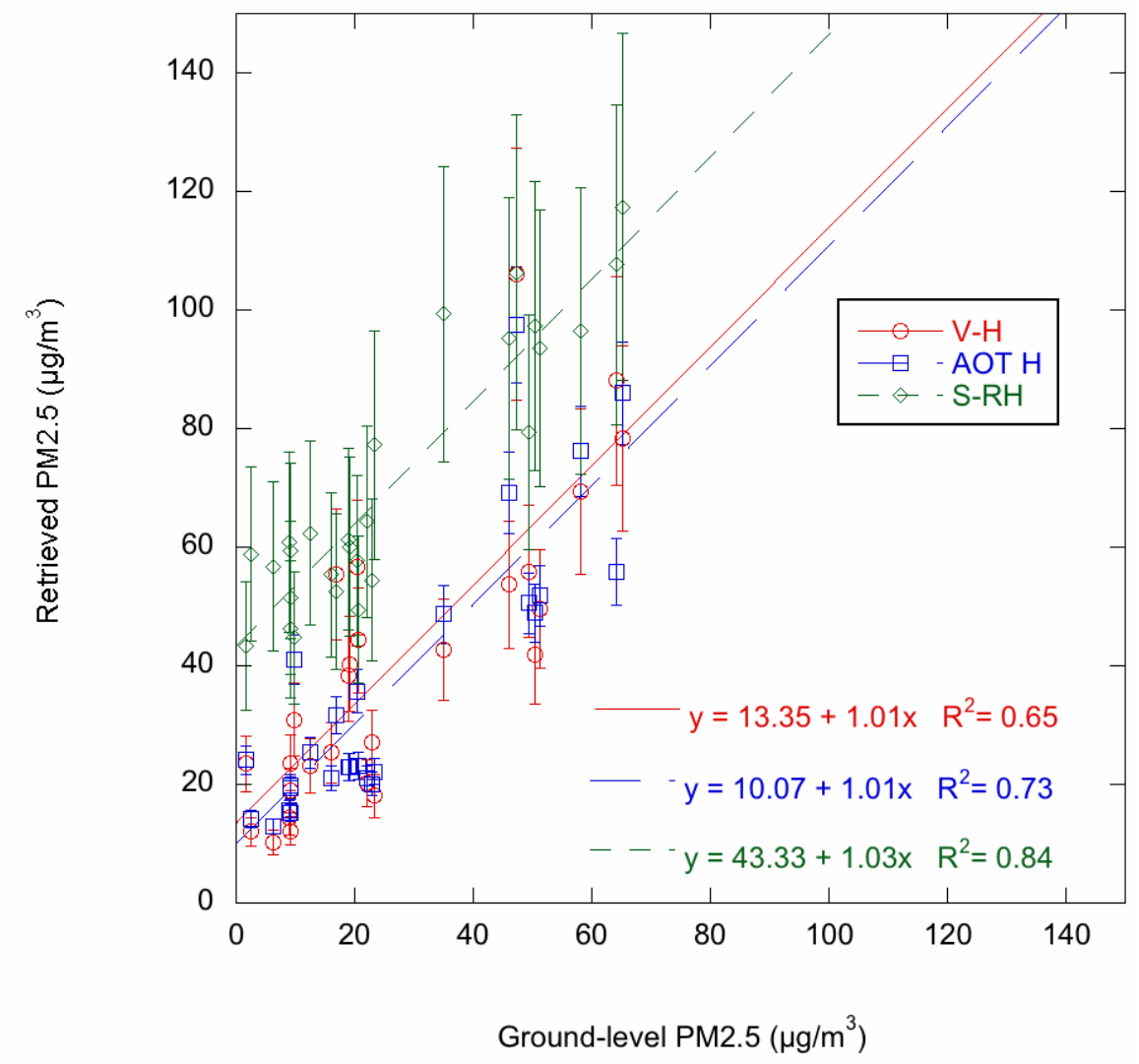

Figure 6. Comparison between ground-level PM2.5 and retrieved PM2.5 using the fine volume fraction (V-H) or the AOT (AOT-H) corrected for the MBL height, and the low level lidar signal (S-RH) corrected for relative humidity effect.